Real-Time Boron Nitride Erosion Measurements of the HiVHAc Thruster via Cavity Ring-Down Spectroscopy

IEPC-2013-119

Brian C. Lee[*] and Azer P. Yalin[†]
Colorado State University, Fort Collins, CO, 80523, USA

Alec Gallimore[‡]
University of Michigan, Ann Arbor, MI, 48109, USA

Wensheng Huang[§] and Hani Kamhawi[¶]
NASA Glenn Research Center, Cleveland, OH, 44135, USA

Cavity ring-down spectroscopy was used to make real-time erosion measurements from the NASA High Voltage Hall Accelerator thruster. The optical sensor uses 250 nm light to measure absorption of atomic boron in the plume of an operating Hall thruster. The erosion rate of the High Voltage Hall Accelerator thruster was measured for discharge voltages ranging from 330 to 600 V and discharge powers ranging from 1 to 3 kW. Boron densities as high as 6.5×10^{15} m^{-3} were found within the channel. Using a very simple boron velocity model, approximate volumetric erosion rates between 5.0×10^{-12} and 8.2×10^{-12} $\frac{m^3}{s}$ were found.

Nomenclature

A_{ki} = Einstein Coefficient
Abs = optical absorbance
c = speed of light in vacuum
d = absorption sample length
f = ring-down ingestion rate
g_i = energy level degeneracy
$k(\nu)$ = absorption coefficient
k_{ij} = deconvolution matrix
l = optical cavity length

[*]Ph.D. Candidate, Physics, Brian.C.Lee6@gmail.com.
[†]Associate Professor, Mechanical Engineering, ayalin@engr.colostate.edu.
[‡]Professor, Aerospace Engineering, alec.gallimore@umich.edu.
[§]Research Engineer, wensheng.huang@nasa.gov.
[¶]Research Engineer, hani.kamhawi-1@nasa.gov.

L_c = single-pass empty cavity loss
N = number density
ν = laser frequency
R = reflectivity of cavity mirror
τ = 1/e decay time, ring-down time
τ_o = 1/e decay time of empty or detuned cavity
$\dot{V}$ = volumetric channel erosion rate

I.   Introduction

Hall thrusters are a type of electric propulsion (EP) device used in space propulsion applications,[1] which were developed initially in the USSR during the 1960s.[2] Hall thrusters offer an attractive combination of high thrust efficiency (>50%), high specific impulse (~1000-3000 s) and, compared to other electric propulsion devices, a high thrust to power ratio. Although less efficient than gridded ion sources, they have higher thrust density allowing for compact propulsion design. These parameters make Hall thrusters suitable for space exploration missions, as well as satellite station keeping and orbit transfer.[3,4] Since their first application in 1971,[2] hundreds of Hall thrusters have been operated in space. Compared to chemical propulsion, Hall thrusters have relatively low thrust (tens of mN to several N), requiring them to be operated for long durations in order to obtain the desired ΔV, and longevity is therefore a critical characteristic.

Despite the widespread use and maturity of Hall thruster technology, there remains a lack of understanding in the plasma physics governing their operation. Of particular interest is the sputter erosion process which slowly erodes the insulating channels walls, eventually leading to device failure. Hall thrusters are designed to last many thousands of hours and the channel erosion rate is slow. The low rate of channel erosion, coupled with the harsh plasma environment within the discharge channel, makes traditional sputter erosion measurements difficult to obtain. This contribution discusses the use of cavity ring-down spectroscopy (CRDS), a sensitive laser-absorption technique, as a novel approach to measure the erosion rate of a Hall thruster *in situ*.

The current paradigm for assessing the lifetime of a Hall thruster is to perform a long duration test, preferably exceeding the length of the targeted mission, which can be many years long. For example, a BPT-4000 Hall thruster was operated for 10,400 hours as part of the flight qualification process.[5] The NEXT ion thruster currently holds the record for the longest duration life test, as it has surpassed 47,000 hours of operation.[6] Such tests occupy vacuum chambers and personnel for long durations, are exceedingly expensive, and severely limit the speed of an iterative design process. A real-time diagnostic tool for assessing Hall thruster erosion lifetime would be exceptionally useful to the electric propulsion community.

Other erosion measurement techniques include profilometry,[7,8] weight loss,[9–11] quartz-crystal microbalance (QCM),[12,13] multilayer coating chip erosion,[14] and optical emission spectroscopy (OES).[15] Profilometry and weight loss measurements require extended thruster run times for significant results, and are difficult to use in parametric studies, in which several thruster operating conditions are to be tested. QCM techniques have the potential to obtain differential sputter yields in relatively short run times, but the harsh thruster environment gives rise to many issues with thermal stability. Multilayer coating chips, which contain tracer materials, can be installed into the thruster channel. The tracer materials are detected as layers of the chip erode with the channel wall. One of the drawbacks of such a method is the need to specially machine and install the multilayer chip into the channel wall. Also, erosion data obtained from observing the chip erosion is highly localized to the chip location. Optical techniques are promising in that they provide real-time erosion data while being non-intrusive and do not require alteration to the thruster. The OES technique observes spontaneous fluorescence of sputter boron atoms in the thruster exhaust plume. OES data is obtained in real time, and is spatially resolved. However, the fluorescence signal is difficult to relate to an absolute boron concentration, as the exact rate of boron excitation is unknown.

Cavity ring-down spectroscopy has exploded in application in recent years.[16,17] CRDS is particularly useful in obtaining absolute trace species concentrations in gas phase. Our past research has shown the possibility of a near real-time sputter sensor for industrial ion beam etch systems,[18] as well as a CRDS sensor for detecting sputtered particles from an anode layer type thruster.[19] The technique has recently been used to measure sputtered atomic boron in the plume of an H6 Hall thruster[20] and an SPT 70.[21] This contribution employs CRDS to measure sputtered atomic boron in the plume of the 3.8 kW HiVHAc thruster.

2

The 33rd International Electric Propulsion Conference, The George Washington University, USA
October 6–10, 2013

The HiVHAc thruster is a long-life thruster which utilizes higher voltages to deliver higher specific impulses. Signifcant work has been done to characterize the operation of the thruster,[22] but further characterization is needed.

The layout of this paper is as follows. Section II describes the CRDS diagnostic technique. Section III gives the experimental setup for the erosion sensor. Section IV gives the results. Section V discusses the erosion measurements, while Section VI gives conclusions.

II. Cavity Ring-Down Spectroscopy Erosion Diagnostic

A. Technique Overview

CRDS is a direct absorption spectroscopy measurement technique that provides extremely high sensitivity by employing enhanced optical-path length. The basic idea of CRDS is to measure the absorption spectrum of a sample (e.g. collection of sputtered particles) that is housed within a high-finesse optical cavity, typically formed from a pair of high-reflectivity mirrors. The laser beam is injected into the optical cavity where it is reflected back and forth many times, e.g. $\sim 10^4$ passes for a mirror reflectivity of R$\approx$0.9999. The intensity of trapped light inside the cavity decays exponentially with time.[16,17] In practice, one can either use a pulsed laser to inject a short pulse of light or, as we do in this work, one can build up light energy in the cavity by illuminating it with a continuous-wave (cw) laser and subsequently extinguishing the laser to yield an exponential decay. A detector placed behind the cavity measures the intensity of light exiting the cavity, which also decays exponentially, yielding the ring-down signal. The exponential decay time constant (also termed ring-down time), τ, is related to the single-pass empty cavity loss L_c, and sample absorbance $Abs(\nu)$ by

$$\frac{1}{\tau(\nu)} = \frac{c}{l}\left(L_c + Abs(\nu)\right) = \frac{1}{\tau_o} + \frac{c}{l}\int_0^d k(x,\nu)\,\mathrm{d}x \tag{1}$$

where c is the speed of light, ν is the laser frequency, l and d are the cavity length and the sample length respectively, x is the position along the optical axis, $k(x,\nu)$ is the absorption coefficient, and τ_0 is the empty cavity ring-down time (often measured by detuning the laser from the sample absorption). The empty cavity loss, L_c, is generally dominated by mirror transmission loss and for a single-pass is then equal to 1-R. When the laser is tuned to resonance with the analyte, there will be additional loss due to absorption, yielding a lower ring-down time.

A commonly used approach for finding a species concentration is to scan the laser frequency across the absorption line and to measure the frequency-integrated spectrum (i.e. the area under the spectral line). Assuming the spectroscopic line parameters are known, the measured area, $\int Abs(\nu)\mathrm{d}\nu$, of a transition from lower state i to upper state k can be readily converted to the path-integrated concentration of the lower state, $\int N_i\mathrm{d}x$ by

$$\int N_i\mathrm{d}x = 8\pi \frac{g_i}{g_k}\frac{v_{ki}^2}{A_{ki}c^2}\left(\int Abs(\nu)\mathrm{d}\nu\right) \tag{2}$$

where g_i, g_k are the level degeneracies, ν_{ki} is the transition frequency, and A_{ki} is the transition Einstein A coefficient.

The path-integrated number densities can be deconvolved using a technique called 'onion-peeling' to show the boron number density as a function of radius along the Hall thruster channel. In the onion-peeling technique, the erosion profile from the thruster is assumed to have azimuthal symmetry, and one divides the thruster into concentric rings with the same spacing as the convolved data. Figure 1 illustrates the onion-peeling technique.

A matrix, k, then relates the path-integrated number densities to the number densities in each ring by the equation

$$k_{ij}N_j(r) = \left(\int N(r)\mathrm{d}x\right)_i \tag{3}$$

where the elements of the matrix k are the path lengths of the beam at position p_j within each ring at radius r_i, and are given by

3

The 33rd International Electric Propulsion Conference, The George Washington University, USA
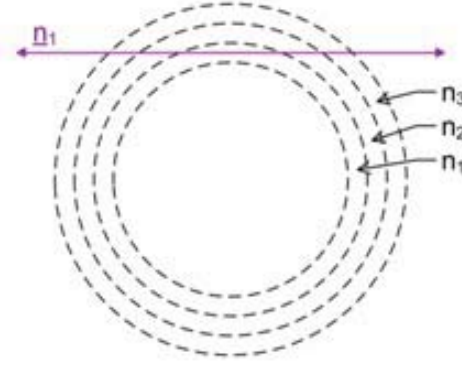*October 6–10, 2013*

Figure 1. Illustration of the onion-peeling technique. The purple line represents the probing laser beam, while the black circles represent the rings of constant boron density.

$$
k_{ij} = \begin{cases}
0, & i < j \\
2\sqrt{r_i^2 - p_j^2}, & i = j \\
2\sqrt{r_i^2 - p_j^2} - 2\sqrt{r_{i-1}^2 - p_j^2}, & i > j
\end{cases}
$$

B. Boron Nitride Detection Scheme

Our approach for detection of boron nitride (BN) is based upon CRDS absorption measurement of sputtered boron atoms. Atomic nitrogen is not a readily optically accessible species. The exact composition of the sputtered particles, i.e. proportions of B, N, B_xN_y etc., is not well understood and may vary with sputtering conditions. Sputter yield measurements indicate the majority of sputtering is in the form of boron and nitrogen atoms, with a very small fraction of B_xN_y clusters.[23] Based on these findings, we assume all sputtering is as atoms, so each sputtered boron atom corresponds to ejection of one boron atom and one nitrogen atom from the BN surface. It is also possible nitrogen sputters as N_2 or N_x, but this does not affect our measurements.
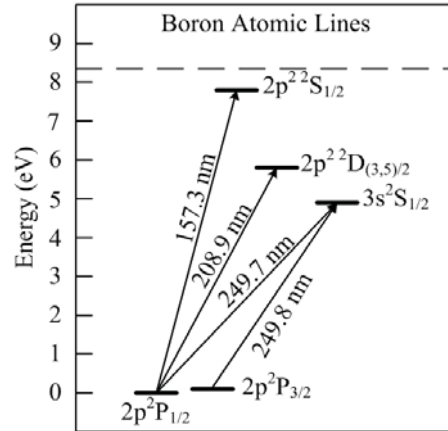

Figure 2. Partial energy diagram for atomic boron.

A partial energy level diagram for neutral boron (B I) is shown in Fig. 2. The ground term has two distinct levels: $2s^2P^0_{1/2}$ (0 eV) and $2s^2P^0_{3/2}$ (0.00189 eV). As a result, fine-structure splitting results in two distinct boron absorption lines near 250 nm: the $2s^2P^0_{1/2} \to 3s^2S_{1/2}$ transition at 249.753 nm (vacuum),

and the $2s^2P_{3/2}^0 \rightarrow 3s^2S_{1/2}$ transition at 249.848 nm (vacuum). Of the two ground state terms, 2/3 of the population will reside in the J=3/2 state. Therefore the J=3/2 ground state transition at 249.848 nm is targeted. The energy level distribution of sputtered boron in a Hall thruster plume is not well understood, and there is no reason to assume *a priori* that the population will follow a Boltzmann distribution. However, the next excited state of boron is at 4.5 eV, and more than 99.9% of the population will reside in the ground state for thermalized populations at wall temperatures even into the thousands of Kelvin.

There are two commonly occurring isotopes of boron: ^{10}B and ^{11}B. The only difference in resonance frequency between the two isotopes is a hyperfine shift, which is small compared to the observed Doppler broadening. The laser therefore interrogates both isotopes simultaneously.

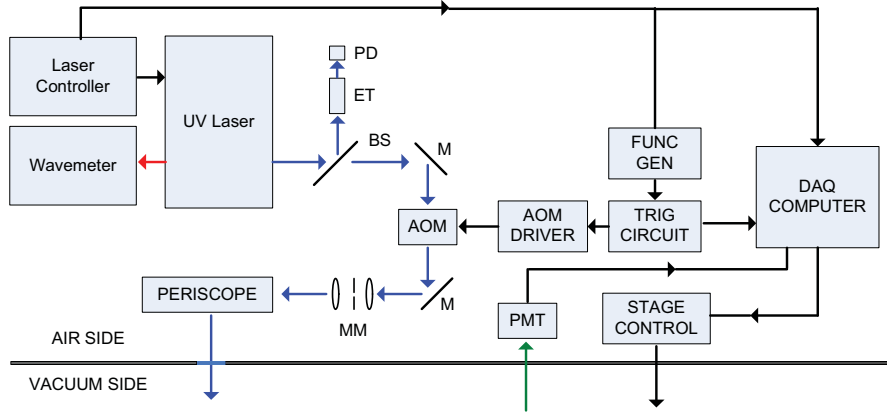## III.   Experimental Setup

A.   Air-side Optical Setup

Figure 3. Diagram of the air-side CRDS experimental setup. PD: Photodiode, ET: Fused Silica Etalon, BS: Beam Splitter, M: Mirror, AOM: Acousto-optic modulator, MM: Mode-match telescope, PMT: Photomultiplier tube.

Figure 3 shows the air-side experimental setup. The laser is a frequency-quadrupled external-cavity diode laser (Toptica, TA-FHG110) producing about 3 mW of continuous-wave UV light, and is capable of scanning the laser frequency >75 GHz. An infrared test beam from the laser is sent into a wavemeter, which is used for coarse wavelength tuning. The beam splitter directs about 10% of the primary-output power through a fused silica etalon that has finesse~20, free-spectral range~2.2 GHz, which is used for fine frequency calibration. As the laser is scanned, the transmission peaks through the etalon are counted, giving a relative frequency calibration. The remainder of the UV laser power goes through an acousto-optic modulator (AOM). The AOM acts as a fast optical switch. When the AOM driver sends RF power to the AOM, the beam is diffracted and directed towards the optical cavity. The AOM driver is turned off, the beam is blocked from the cavity.

A pinhole is placed in the middle of a mode-matching telescope. The pinhole acts as a spatial filter, ideally only allowing the $TEM_{0,0}$ mode through to the cavity. The mode-match lens is specifically placed to match the beam waist to the fundamental transverse mode of the cavity. Details of mode-matching can be found in Kogelnik and Li.[24] A periscope brings the beam up to the height of the vacuum chamber and through an input window to the detection cavity. The light from the output fiber is detected by a photomultiplier tube.

A custom-made trigger circuit continuously monitors the signal from the PMT and compares it to the trigger level. When the signal from the cavity exceeds the trigger level, the trigger circuit will turn off the AOM driver and trigger the data acquisition (DAQ) computer to record the PMT signal. A function generator continuously adjusts the trigger level to account for the changing laser power as the laser is scanned in frequency. When the DAQ computer is triggered, a high-speed DAQ card digitizes the ring down at a rate of 10^8 samples/sec. At the same time, a slow DAQ card records the laser frequency. Each digitized ring down is fit to an exponential. The ring-down time and its associated laser frequency form the function $\tau(\nu)$ from Eqn. 1. After recording a given number of ring-down events, the DAQ computer moves the thruster

5

The 33rd International Electric Propulsion Conference, The George Washington University, USA
October 6–10, 2013

stage in order to record erosion at a different position on the thruster.

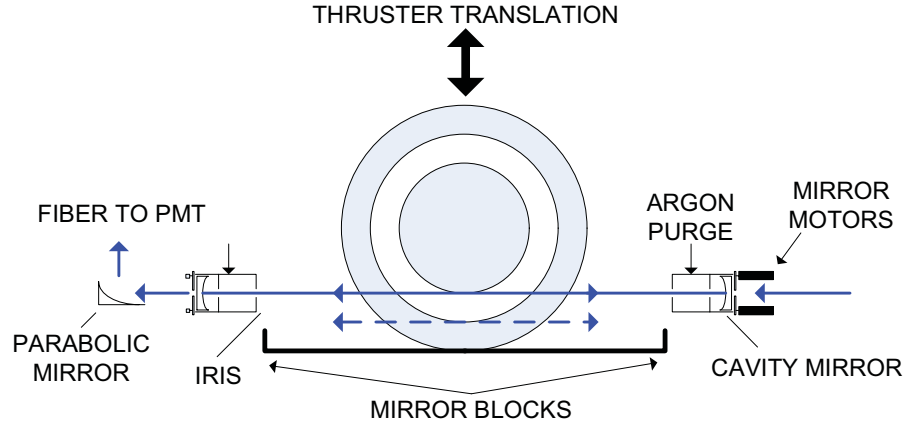## B.   Vacuum-side Optical Setup

Figure 4.   Diagram of the vacuum-side optical setup. The two cavity mirrors form the high-finesse optical cavity, with the optical axis 6 mm downstream of the thruster exit plane. The solid line corresponds to a beam position of P=0, while the dashed line corresponds to P=1.

Figure 4 shows a diagram of the vacuum-side experimental setup. The interrogating laser beam enters through the chamber window from the right. A 54 cm long optical cavity is formed by a pair of high reflective mirrors (R=99.75%, MLD Technologies). The axis of the cavity is parallel to the exit plane of the thruster, and is 6 mm downstream from the exit. Each mirror is placed on an optical mount, allowing for fine adjustment of the mirrors. The first cavity mirror mount has two motorized actuators, allowing for cavity adjustment while under vacuum. Light exiting the optical cavity is focused into a 500 μm diameter core fiber for detection using an off axis parabolic mirror.

In front of each mirror are two 3 mm diameter irises for the laser to pass through. The mirrors are sealed off from the thruster plasma with the exception of the two holes for the beam. Exposure to the thruster plasma causes degradation in the mirror performance. The irises serve to block as much plasma exposure as possible. Additionally, a 1 sccm argon purge flow is introduced in front of each mirror. The argon fills the volume in front of the mirrors, creating a region with a mean free path of ∼1 cm, which serves to deflect sputtered particles from streaming directly to the mirror surfaces and coating the mirrors. Two mirrors covers are attached to the translation stage. While the thruster is operating, but the optical sensor is not being used, the thruster can be translated up, and the mirror covers block the irises, thereby minimizing the mirror degradation during thruster bake out. The thruster was operated for over 11 hrs, resulting in the mirrors degrading from 99.82% reflectivity to 99.55%, corresponding to a factor of ∼2.5 drop in optical sensitivity.

C.   Thruster and Vacuum Facility

The HiVHAc thruster was operated in NASA Glenn's VF8 facility, which is an entirely oil diffusion pumped chamber with a 1.5 m diameter and ∼ 5.5 m length. The chamber base pressure is ∼ 4×10^{-7} torr. With 41 sccm of Xe flowing, the background pressure is ∼ 1×10^{-5} torr (corrected for Xe). The thruster was mounted onto a vertical motorized translation stage, allowing boron spectra to be obtained at different positions along the thruster exit plane. Throughout this paper, the relative position of the thruster and laser beam will be reported in the non-dimensional P unit. When path-integrated boron densities are reported, the non-dimensional beam position is used, and refers to the location of the laser beam relative to the thruster. The solid blue line in Fig. 4 corresponds to $P=0$, i.e. where the laser beam is tangent to the inner channel wall. The dashed blue line shows the $P=1$ coordinate, where the laser is tangent to the outer channel wall. When absolute boron densities are reported, the non-dimensional coordinate refers to the thruster radius. A radius of $P=0$ is the radius of the inner channel wall, while $P=1$ is the radius of the outer channel wall. Note

that in this system coordinate, the thruster center has a negative P value. Figure 5 shows a picture of the HiVHAc thruster and the optical support structure within VF8.
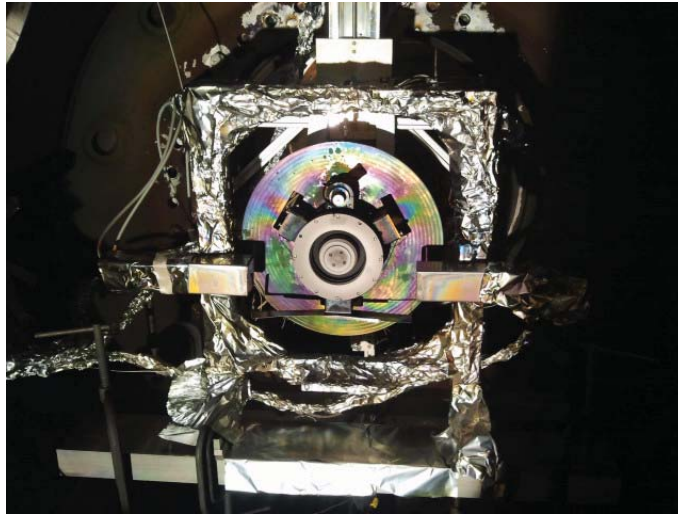

Figure 5. Picture of the HiVHAc thruster and CRDS setup within the VF8 chamber. The optical frame was wrapped in 3 layers of foil to help reduce misalignment induced by heating.

IV. Results

Figure 6 shows representative boron absorption spectra with the thruster running at 500 V discharge voltage and 2 kW discharge power. The laser frequency was continuously swept across the boron resonance. The horizontal axis gives the relative laser frequency (i.e. the 0 point is arbitrary). In this particular case, the center of the boron resonance was near 0.4 cm^{-1}. The 250 nm laser cannot scan sufficiently far in frequency to capture the entire spectrum. In order to differentiate between empty-cavity loss and boron absorption, it is necessary to capture both the center of the absorption peak and one side of the baseline. For this reason, the center of the laser scan was intentionally offset from the center of the boron resonance. For each spectrum, 5,000 ring-downs were recorded.
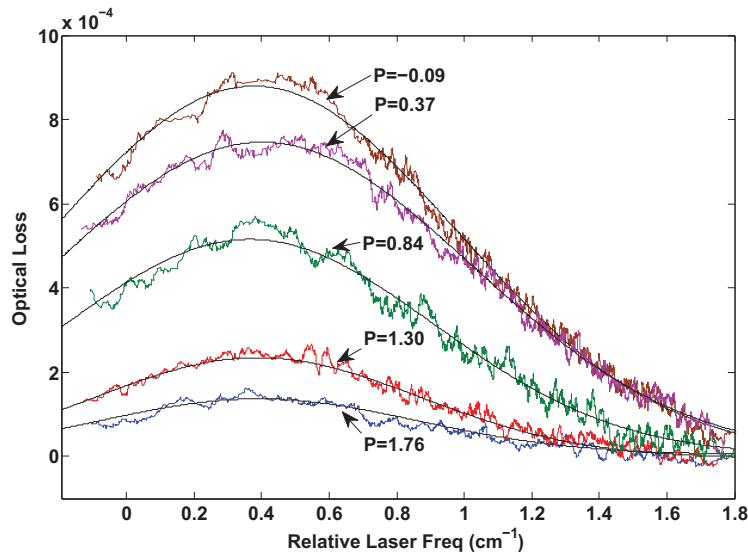

Figure 6. Representative boron absorption spectra for the 2 kW, 500 V thruster condition. The different spectra are at different positions along the thruster channel. The black lines are Gaussian fits.

7

The 33rd International Electric Propulsion Conference, The George Washington University, USA
October 6–10, 2013

Although the spectral broadening is entirely due to Doppler shifting, there is no reason to assume a Gaussian velocity distribution. Nevertheless, a Gaussian fits the data very well, and is used to compute the total area under the spectral curve (the value $\int Abs(\nu)d\nu$). Equation 2 then yields the path-integrated boron density (i.e. the integral of the boron density along the laser path).

Figure 7 shows the path-integrated boron number densities as a function of channel position. The thruster was held at 500 V, while the power set points were 1, 1.5, 2, 2.5 and 3 kW. At each setpoint, data was not taken until the discharge current had stabilized.
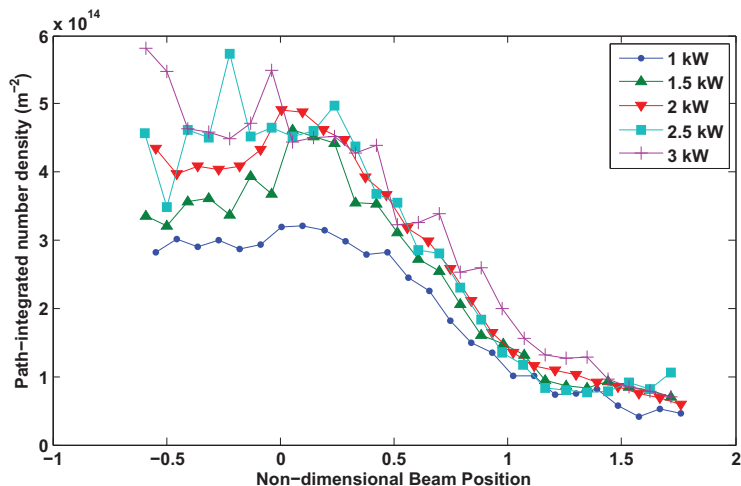

Figure 7. Path-integrated boron number densities as a function of channel position. The thruster was held at 500 V for each condition.

Figure 8 gives the same information as Fig. 7, except that the power was held at 2 kW, while the discharge voltage was varied.
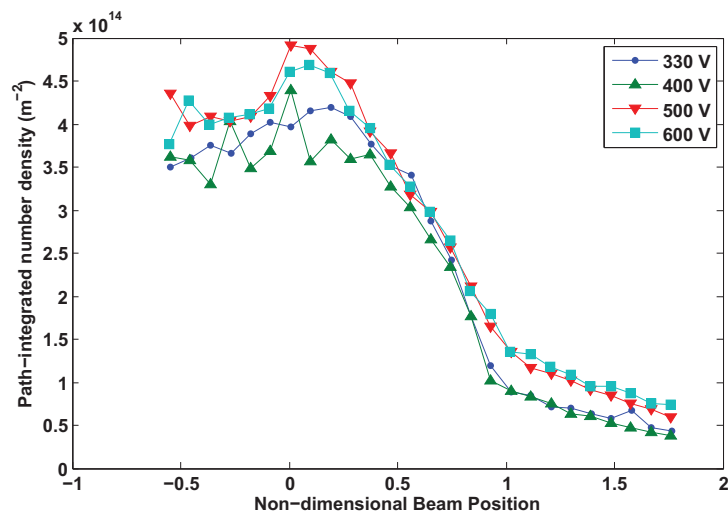

Figure 8. Path-integrated boron number densities as a function of channel position. The thruster was held at 2 kW for each condition.

The sensor showed good repeatability. The 2 kW, 500 V thruster condition was measured at the beginning and end of testing and is shown in Fig. 9.

8

The 33rd International Electric Propulsion Conference, The George Washington University, USA
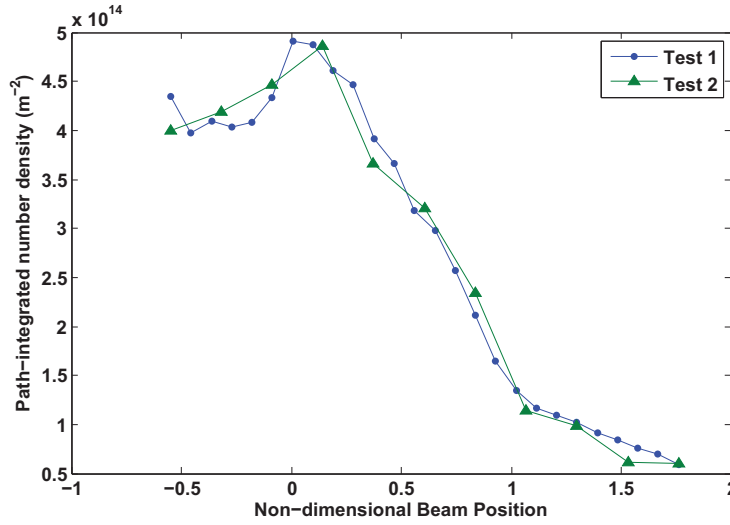*October 6–10, 2013*

Figure 9. The 2 kW, 500 V condition was measured at the beginning and end of testing and showed good repeatability.

The path-integrated values for each of the thruster conditions can then be deconvolved using the onion peeling method described earlier to yield boron number densities (that are not path integrated) as a function of thruster radius. The deconvolved data is shown in Fig. 10 and Fig. 11
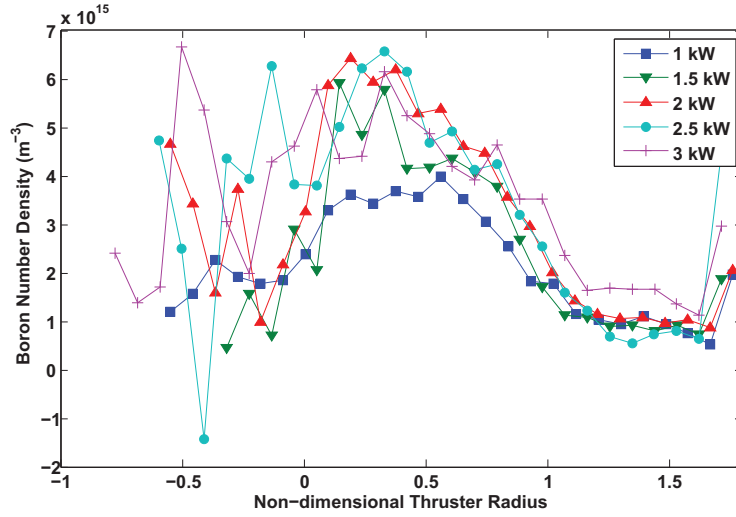

Figure 10. Boron number densities as a function of channel position. The thruster was held at 500 V for each condition.

9

The 33rd International Electric Propulsion Conference, The George Washington University, USA
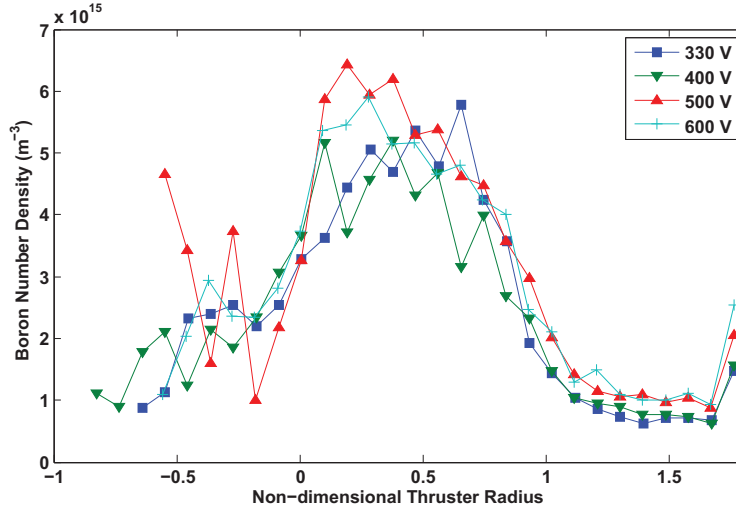*October 6–10, 2013*

Figure 11. Boron number densities as a function of channel position. The thruster was held at 2 kW for each condition.

Each path-integrated boron density value was computed from the area under a Guassian fit. The fit coefficients had associated 95% confidence intervals, which were propagated through the calculations to find path-integrated number density, as well as through the matrix deconvolution process to find number density. Figure 12 and Fig. 13 show the resulting error bars for the 2 kW, 600 V case, which are representative of other cases. Systematic error sources exist as well, some of which are discussed in the next section.
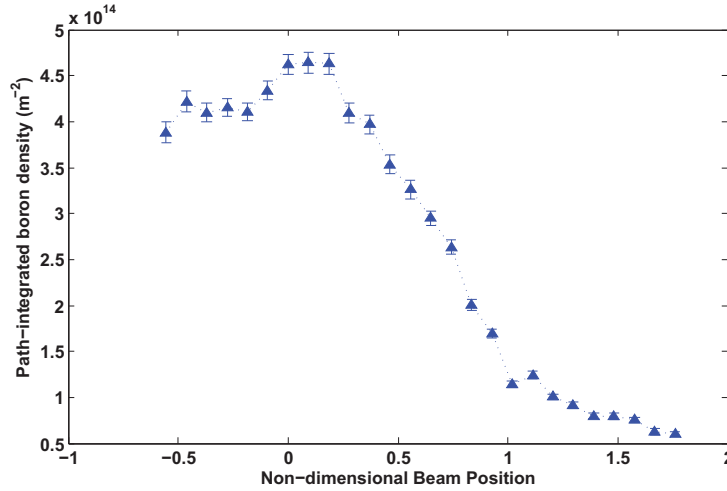

Figure 12. Path-integrated boron number density for the 2 kW, 600 V thruster setpoint showing representative 95% confidence intervals.
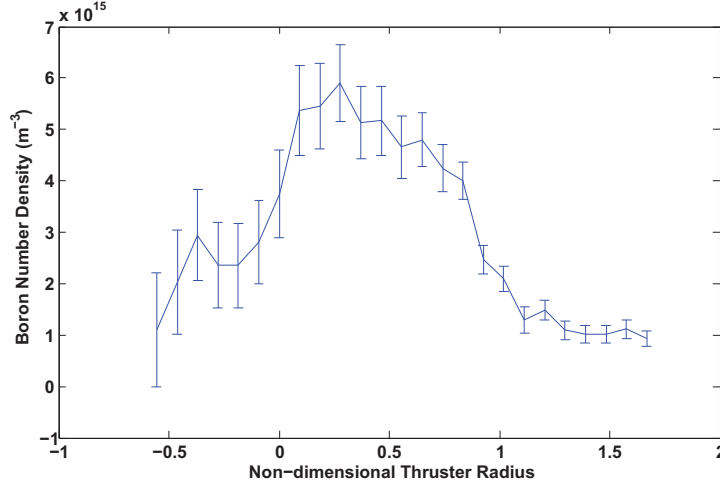
Figure 13. Deconvoled boron number density for the 2 kW, 600 V thruster setpoint showing representative 95% confidence intervals.

V.   Discussion

To obtain the boron flux from the thruster, each boron number density needs to be multiplied by the average boron velocity perpendicular to the optical axis. These velocities are not yet well known. However, we can estimate a characteristic velocity from the laser-induced fluorescence (LIF) done by Tao and Yalin.[25] Tao used LIF to measure the flux-based Sigmund-Thompson velocity distribution given by

$$f(u) = C \frac{u^3}{(u^2 + v_b^2)^{3-2m}} \tag{5}$$

where u is the boron speed and v_b and m are fit constants found to be 9,500 m/s and 0.17 respectively. A characteristic boron velocity can be found by averaging the Sigmund-Thompson distribution, which yields 23 km/s. However, this value is very sensitive to the exact values of v_b and m, as well as the limits of integration used. The Doppler broadening observed in the boron spectra gives the velocity profile parallel to the optical axis. While the velocity component perpendicular to the optic axis is needed, the parallel component gives some insight into a typical boron velocity. The spectra have a typical Doppler broadened width of ~ 0.8 cm^{-1}, which corresponds to a velocity of ~ 6 km/s. Work is underway to both directly measure and to model the needed velocity profiles within an operating Hall thruster. For an approximation, we will assume an average boron velocity of 10 km/s perpendicular to the optical axis.

The flux of boron atoms at each point along the channel is found from the product of the boron number density and velocity. Integrating the boron flux over the thruster exit area (assuming azimuthal symmetry) yields the total flux of boron atoms. As per Section 2.B, we assume that for every boron atom ejected from the channel, one nitrogen is ejected, and no $B_x N_y$ compounds. Therefore, the volumetric channel erosion rate is given by

$$\dot{V} = \frac{m_{BN}}{\rho_{BN}} \left(\frac{g_{1/2} + g_{3/2}}{g_{3/2}} \right) \Phi_{3/2} \tag{6}$$

where m_{BN} is the mass of one boron and one nitrogen, ρ_{BN} is the density of boron nitride, $g_{1/2}$ and $g_{3/2}$ are the level degeneracies of the two boron ground states, and $\Phi_{3/2}$ is the total boron flux in the $J=3/2$ level (i.e. boron atoms per second in the J=3/2 state).

Under the boron velocity assumptions mentioned above, the volumetric erosion rate of the boron nitride channel is given for each thruster condition in Table 1. For comparison, the erosion rate of the 660 W SPT-70 was found, using the same technique, to be $\sim 3 \times 10^{-13}$ m^3/s. The results are also summarized in Fig. 14 and Fig. 15. As discussed above, the reported uncertainties are from statistical noise only.

Table 1. Volumetric erosion rates for each thruster condition.

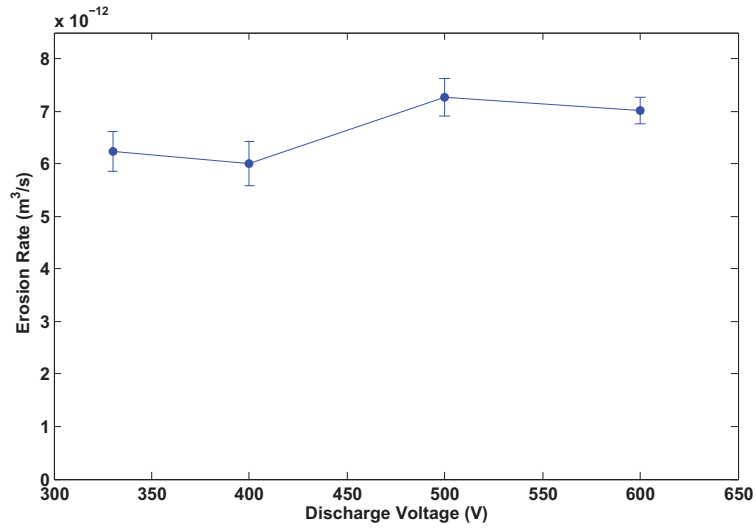| Power (kW)	Voltage (V)	Erosion Rate $\left(\frac{m^3}{s}\right)$	% Statistical Uncertainty
1	500	5.08×10^{-12}	5.0
1.5	500	5.48×10^{-12}	5.5
2	330	6.24×10^{-12}	6.0
2	400	6.01×10^{-12}	7.0
2	500	7.27×10^{-12}	5.0
2	600	7.01×10^{-12}	3.6
2.5	500	7.21×10^{-12}	12
3	500	8.23×10^{-12}	9.0

Figure 14. Channel volumetric erosion rates for varying discharge voltage with a constant 2 kW power.
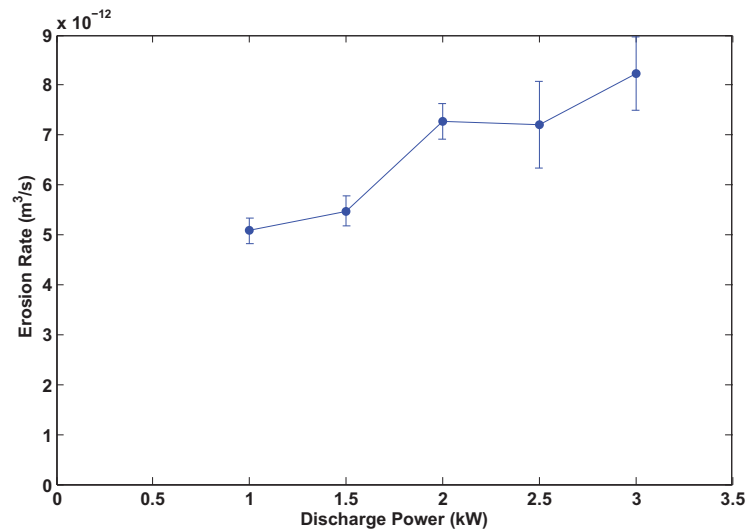

Figure 15. Channel volumetric erosion rates for varying discharge power with a constant 500 V discharge voltage.

As mentioned in Section 2.B, the CRDS sensor probes ground state neutral boron. Any fraction of the boron population which is ionized or electronically excited, is not counted. Uncertainty remains in the exact fraction of boron population which resides in the neutral ground state. Estimates of the fraction of boron population which is ionized have been made. Electron-impact ionization cross sections were calculated using methods from Gryzinski.[26] The ionization cross sections are functions of incident particle energy (i.e. electron speed). First, an average cross-section is found by

$$< \sigma >= \frac{2}{\sqrt{\pi}} \left(k_B T_e\right)^{-3/2} \int_0^\infty \sqrt{E} e^{\frac{-E}{k_B T_e}} \sigma(E) \mathrm{d}E \tag{7}$$

and is used to compute the ionization mean free path

$$MFP = \frac{1}{n_e < \sigma >} \tag{8}$$

where E is the energy of the incident electron, k_B is Boltzmann's constant, T_e is the electron temperature, σ is the ionization cross section, and n_e is the electron density. For example, for T_e=10 eV, and $n_e = 10^{12}$ cm^{-3}, the mean free path is found to be 54 cm. Table 2 gives ionization population fractions for estimated electron temperatures and densities, assuming the boron atoms have to travel ∼3 cm before reaching the interrogating laser. No internal diagnostics have been performed on HiVHAc, so a range of likely values is considered. As can be seen in Table 2, the estimated error caused by ionized boron could be fairly small, or quite significant. Additionally, any neutral boron which is not in the ground state will not be counted. However, excited population fraction is not known, and estimates have not yet been made. There is a 3 % uncertainty in the fundamental boron transition line coefficients[27] used to compute the path-integrated boron number density.

Table 2. Estimated percent ionized boron after traveling 3 cm.

$T_e(eV)$	$n_e(cm^{-3})$ 10^{11}	10^{12}	10^{13}
10	0.6	5.4	43
20	1.2	11	68
30	1.5	14	78

Note that denser and more energetic plasmas will ionize and excite sputtered boron atoms over shorter distances, thus causing a lower fraction of the boron population to be counted. As the thruster power is increased, a lower fraction of the boron may be counted, skewing the observed erosion rate versus discharge power.

The measured trends in erosion rate are difficult to interpret. Of course, systematic errors exist in the measurement technique itself, some of which were discussed earlier. Provided the observed trends are physical, two things stand out. First, at constant power, the erosion did not change significantly with voltage. Second, while the erosion rate increased roughly linearly with discharge power at constant voltage, the trend does not pass through the origin.

In erosion studies[20] of the H6 thruster, the erosion rate was seen to scale as $I_d V_d^2$. In the H6 thruster, the acceleration zone was observed to move upstream as the discharge voltage increased, causing the erosion zone length to increase, and increasing the potential drop between the plasma and channel wall. However, the HiVHAc thruster may not behave in a similar way. The acceleration zone could move downstream with increasing voltage or flow rate, thus causing little change in erosion rate.

VI.   Conclusions

We have demonstrated use of a CRDS erosion sensor to measure the real-time boron nitride erosion rate from the HiVHAc thruster. Measured boron densities showed excellent repeatability from the beginning to the end of the test. No strong trend was found between the channel erosion rate and the discharge voltage for constant power. The erosion rate increased roughly linearly with discharge power, however, the trend did not appear to pass through the origin, as expected. Preliminary hypotheses for these trends were discussed.

The velocity model used to compute the volumetric flux rate is very approximate. Future work includes comparison with high-fidelity models which simulate both the erosion rate as well as the velocity distribution of the sputtered boron. Additionally, laser-induced fluorescence experiments are planned, which will directly measure the velocity distribution of the sputtered boron.

Acknowledgments

References

[1]Kaufman, H. R., "Technology of closed-drift thrusters," *AIAA Journal*, Vol. 23, No. 1, Jan. 1985, pp. 78–87.

[2]Kim, V., Kozubsky, K., Murashko, V. M., and Semenkin, A., "History of the Hall Thrusters Development in USSR," *30th International Electric Propulsion Conference*, No. IEPC-2007-142, Florence, Italy, 2007.

[3]Oleson, S. R., Myers, R. M., Kluever, C. A., Riehl, J. P., and Curran, F. M., "Advanced Propulsion for Geostationary Orbit Insertion and North-South Station Keeping," *Journal of Spacecraft and Rockets*, Vol. 34, No. 1, Jan. 1997, pp. 22–28.

[4]Dankanich, J., Drexler, J., and Oleson, S., "Electric Propulsion Mission Viability within the Discovery Class Cost Cap," *46th AIAA/ASME/SAE/ASEE Joint Propulsion Conference & Exhibit*, No. AIAA-2010-6776, Nashville, TN, 2010.

[5]Grys, K. D., Mathers, A., Welander, B., and Khayms, V., "Demonstration of 10,400 Hours of Operation on 4.5 kW Qualification Model Hall Thruster," *46TH AIAA/ASME/SAE/ASEE JOINT PROPULSION CONFERENCE & EXHIBIT*, No. AIAA-2010-6698, Nashville, TN, 2010.

[6]Shastry, R., Herman, D., Soulas, G., and Patterson, M., "NASA's Evolutionary Xenon Thruster (NEXT) Long-Duration Test as of 736 kg of Propellant Throughput," *48th AIAA/ASME/SAE/ASEE Joint Propulsion Conference & Exhibit*, No. AIAA-2012-4023, Atlanta, Georgia, 2012.

[7]Peterson, P. Y. and Manzella, D. H., "Investigation of the Erosion Characteristics of a Laboratory Hall Thruster," *39th AIAA/ASME/SAE/ASEE Joint Propulsion Conference & Exhibit*, No. AIAA-2003-5005, Huntsville, Alabama, 2003.

[8]Misuri, T., Milani, A., and Andrenucci, M., "Development of a Telemicroscopy Diagnostic Apparatus and Erosion Modelling in Hall Effect Thrusters," *31st International Electric Propulsion Conference*, No. IEPC-2009-036, Ann Arbor, Michigan, 2009.

[9]Garnier, Y., Viel, V., Roussel, J.-F., and Bernard, J., "Low-energy xenon ion sputtering of ceramics investigated for stationary plasma thrusters," *Journal of Vacuum Science & Technology A: Vacuum, Surfaces, and Films*, Vol. 17, No. 6, 1999, pp. 3246.

[10]Yalin, A. P., Surla, V., Farnell, C., Butweiller, M., and Williams, J. D., "Sputtering Studies of Multi-Component Materials by Weight Loss and Cavity Ring-Down Spectroscop," *42nd AIAA/ASME/SAE/ASEE Joint Propulsion Conference & Exhibit*, No. AIAA-2006-4338, Sacramento, California, 2006.

[11]Rubin, B., Topper, J. L., and Yalin, a. P., "Total and differential sputter yields of boron nitride measured by quartz crystal microbalance," *30th International Electric Propulsion Conference*, No. IEPC-2007-074, Florence, Italy, 2007.

[12]Pagnon, D., Balika, L., and Pellerin, S., "QCM and OES: two ways used to study simultaneously HET thruster chamber ceramic erosion. First QCM results on PPS100-ML validate previous OES measurements." *31st International Electric Propulsion Conference*, No. IEPC-2009-118, Ann Arbor, Michigan, 2009.

[13]Rubin, B., Topper, J. L., Farnell, C. C., and Yalin, a. P., "Quartz crystal microbalance-based system for high-sensitivity differential sputter yield measurements." *The Review of scientific instruments*, Vol. 80, No. 10, Oct. 2009, pp. 103506.

[14]Cho, S., Yokota, S., Hara, K., Takahashi, D., Arakawa, Y., Komurasaki, K., and Kobayashi, A., "Hall Thruster Channel Wall Erosion Rate Measurement Method Using Multilayer Coating Chip," *46th AIAA/ASME/SAE/ASEE Joint Propulsion Conference & Exhibit*, No. AIAA-2010-6697, Nashville, TN, 2010.

[15]Celik, M., Batishchev, O., and Martinez-Sanchez, M., "Use of emission spectroscopy for real-time assessment of relative wall erosion rate of BHT-200 hall thruster for various regimes of operation," *Vacuum*, Vol. 84, No. 9, April 2010, pp. 1085–1091.

[16]Berden, G., Peeters, R., and Meijer, G., "Cavity ring-down spectroscopy: Experimental schemes and applications," *International Reviews in Physical Chemistry*, Vol. 19, No. 4, Oct. 2000, pp. 565–607.

[17]Paldus, B. A. and Kachanov, A. A., "An historical overview of cavity-enhanced methods," *Canadian Journal of Physics*, Vol. 83, 2005, pp. 975–999.

[18]Tao, L., Yalin, A. P., and Yamamoto, N., "Cavity ring-down spectroscopy sensor for ion beam etch monitoring and end-point detection of multilayer structures." *The Review of scientific instruments*, Vol. 79, No. 11, Nov. 2008, pp. 115107.

[19]Yamamoto, N., Tao, L., Rubin, B., Williams, J. D., and Yalin, A. P., "Sputter Erosion Sensor for Anode Layer-Type Hall Thrusters Using Cavity Ring-Down Spectroscopy," *Journal of Propulsion and Power*, Vol. 26, No. 1, Jan. 2010, pp. 142–148.

[20]Huang, W., Gallimore, A. D., and Smith, T. B., "The Technical Challenges of using Cavity Ring-Down Spectroscopy to Study Hall Thruster Channel Erosion," *32nd International Electric Propulsion Conference*, No. IEPC-2011-030, Wiesbaden, Germany, 2011.

14

The 33rd International Electric Propulsion Conference, The George Washington University, USA
October 6–10, 2013

[21]Lee, B. C., Taylor, J. M., Leach, R. W., and Yalin, A. P., "Boron Nitride Erosion Measurements of an SPT-70 Hall Thruster via Cavity Ring-Down Spectroscopy," *6th Spacecraft Propulsion Meeting, Joint Army-Navy-NASA-Air Force*, No. 3137, Colorado Springs, CO, 2013.

[22]Huang, W., Kamhawi, H., and Shastry, R., "Farfield Ion Current Density Measurements before and after the NASA HiVHAc EDU2 Vibration Test," *48th AIAA/ASME/SAE/ASEE Joint Propulsion Conference & Exhibit*, No. AIAA-2012-4195, Atlanta, Georgia, 2012.

[23]Rubin, B., Topper, J. L., and Yalin, A. P., "Total and differential sputter yields of boron nitride measured by quartz crystal microbalance," *Journal of Physics D: Applied Physics*, Vol. 42, No. 20, Oct. 2009, pp. 205205.

[24]Kogelnik, H. and Li, T., "Laser beams and resonators," *Proceedings of the IEEE*, Vol. 54, No. 10, 1966, pp. 1312–1329.

[25]Tao, L., Yalin, A., and Collins, F., "Velocity Profiles of Boron Atoms Sputtered from Boron Nitride by Low Energy Xenon Ions," *32nd International Electric Propulsion Conference*, No. IEPC-2011-067, Wiesbaden, Germany, 2011.

[26]Gryzinski, M., "Classical Theory of Atomic Collisions. I. Theory of Inelastic Collisions," *Phys. Rev.*, Vol. 138, Apr 1965, pp. A336–A358.

[27]Kramida, A., Yu. Ralchenko, Reader, J., and and NIST ASD Team, NIST Atomic Spectra Database (ver. 5.1), [Online]. Available: `http://physics.nist.gov/asd` [2013, September 18]. National Institute of Standards and Technology, Gaithersburg, MD., 2013.